Comparisons of Methods in Near-to-Far-Field Transformations for Waveguides

David Dong

Under the direction of

Rordrigo Arrieta
MIT Department of Mathematics

Research Science Institute
August 1, 2023

Abstract

A fundamental problem in exterior scattering theory is to determine the most accurate and computationally simple method to model the scattered field produced by an incoming electromagnetic wave that diffracts off a surface like a perfect electrical conductor. This paper focuses on improving the accuracy of the underlying methods specifically on unbounded scatters, by evaluating the field produced by every point on an imaginary surface. We explore two new methods to accurately compute the electric scatter resulting from these individual points. The first method utilizes the recently developed windowed Green's function, and the second method uses a perfectly matched layer on the same infinite imaginary surface. We analyze, both numerically and through asymptotics, the errors resulting from these two methods under fixed conditions.

Summary

One fundamental problem in physics and electrical engineering is how to compute and model electromagnetic fields, both theoretically and numerically. This is required, for instance, when trying to model the scatter of electromagnetic waves off an antenna in satellite communications. In our paper, we compute the electric field in a two dimensional surface where we make several assumptions: the plane is empty space except for a single conductor extending infinitely in one direction, with a single point radiating out electromagnetic waves. We analyze two new methods to compute the electric field at far away points, known as a windowed Green's function and a perfectly matched layer, both of which are based off of writing an incoming electromagnetic wave as the sum of many waves on the surface of a conductor. We provide bounds on the errors of these method and evaluate their performance against each other in practical simulations.

1 Introduction

In computational electromagnetism we often need to determine how a surface like an antenna would scatter incoming electromagnetic waves. To do this we use Maxwell's equations to model the electric and magnetic fields. Such a problem lies in the domain of *exterior scattering theory* [6].

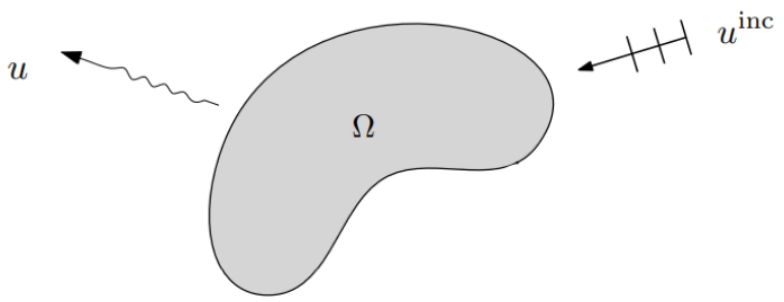

Figure 1: An example exterior scattering theory problem. Some incoming electromagnetic wave, u^{inc} hits a surface Ω like an antenna, leading to a diffracted field u.

For any given surface and initial conditions, there are several techniques that have been developed that can be used to solve the situation given in Figure 1 numerically. The simplest one is the *finite difference method* (FDM), which in two dimensions chooses a rectangle inside the plane and approximates Maxwell's equation on each point.This allows us to reduce a differential equation into a system of linear equations [11]. The similar *finite element method* (FEM) breaks the plane down into smaller, arbitrary, surfaces known as finite elements, and solves the differential equation in each surface [12]. One final method is known as the *boundary integral equation* method, which uses *Green's representation theorem*, representing the electric field as a sum of radiating waves on the boundary of the surface, allowing us to compute the magnitude of the electromagnetic field at every point with an integral over the surface [3, 8]. Each of these three methods have advantages and disadvantages, based on context.

In particular, in exterior scattering theory we often need to determine the magnitude of waves very far from our surface. This makes the FDM and the FEM impractical, because it is impossible to discretize an infinite surface. In these cases, we can instead perform a *near-to-far-field transformation*, where we first use a method to determine the field at close points, and then apply Green's representation theorem on an imaginary surface close to the real surface. This allows us to determine the magnitude of the electric or magnetic field at any point given the field at close points [16].

In many cases we also need to analyze the effects of an incoming electromagnetic field on a surface that can be approximated as *infinite*, like a waveguide [5]. In these situations, the surface is often truncated so that Green's representation theorem can be applied. However, such methods often compromise accuracy significantly because electric fields decay very slowly, and are oscillatory, leading to large errors in the approximation of Green's

representation theorem [1]. Furthermore, in layer media problems, this truncation increases computation time, as we must evaluate complicated Sommerfeld integrals [5].

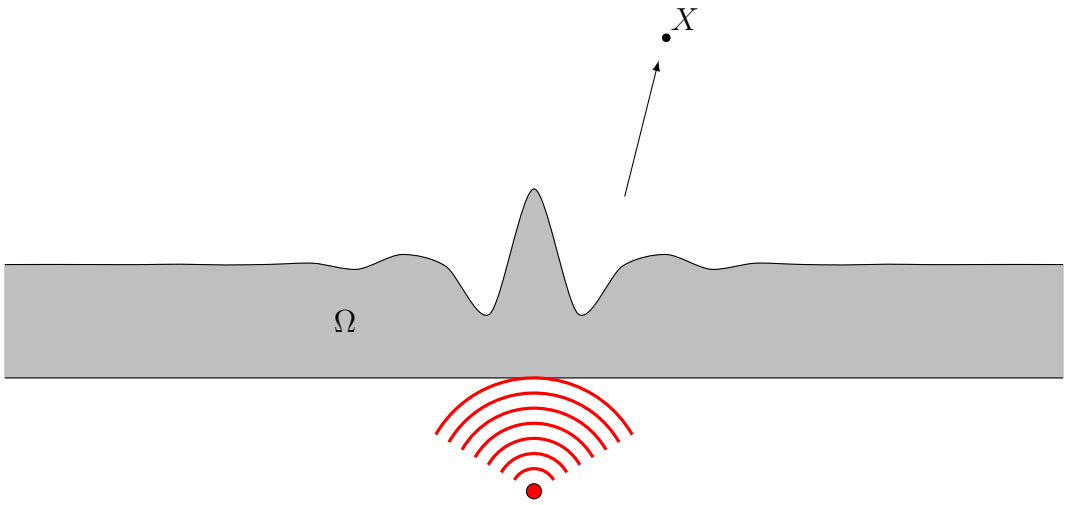

Figure 2: An example infinite waveguide, labeled Ω, with a perturbation of the surface of the waveguide (as if the real-life cable was misshapen). There is a single source of electromagnetic waves radiating from the red point. We wish to determine the magnitude of the electric field at an arbitrary point X that may be very far away from the waveguide.

Several techniques have been developed to reduce error in exterior scattering problems, including a windowed Green's function and a perfectly matched layer. However, neither perfectly matched layers nor the windowed Green's function were originally developed for near-to-far-field transformations. We will be applying both to near-to-far-field transformations involving infinite surfaces.

Perfectly matched layers (PMLs) were originally developed to approximate an infinite surface in finite difference and finite element methods. This technique sends a part of the discretized surface near the perimeter into the complex plane [4]. Without a PML, electromagnetic waves bounce off the discretized surface, leading to errors. These reflections get "absorbed" by a PML, quickly going to zero outside of the main surface. Recently, PMLs have recently been applied to boundary integral equations contexts [14].

Windowed Green's function (WGFs) were originally developed for boundary integral equations in layered media [5]. They add a weight ranging from 0 to 1 in the integral computed for Green's representation theorem, smoothing out the errors caused in truncating a oscillating electric field. The function also avoids having to compute numerically the complicated Sommerfeld integrals in layer media problems [5]. The technique was first applied to scattering theory in layered media [5]. However, it has since been applied to scattering theory with waveguides [1, 2].

In our paper, we extend the idea of WGFs and PMLs by applying these methods in a near-to-far-field context with an unbounded waveguide. We then compare the error between these two methods under various conditions.

Our paper is organized as follows. In Section 2, we develop the mathematics required for our paper, explaining past efforts in scattering theory to solve the Helmholtz equation.

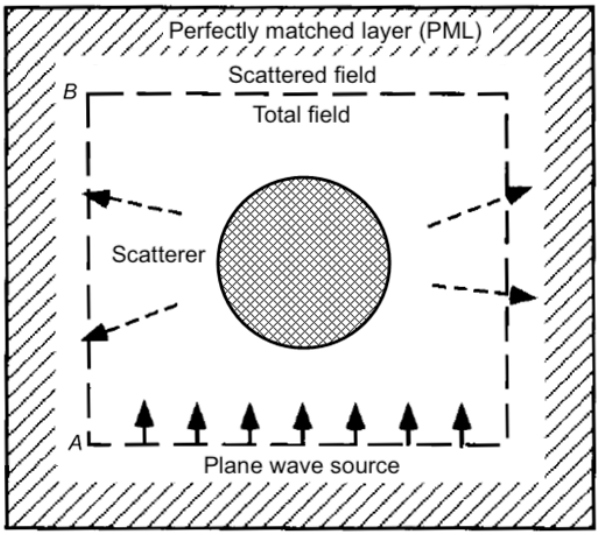

Figure 3: An example of an area where a perfectly matched layer is applied to a finite difference method, in order to decrease scattering on the boundary of the discretized surface. [7]

This includes topics relating to Green's function and perfectly matched layers. Then, in Section 3, we develop theory that will allow us to asymptotically analyze perfectly matched layers in comparison to windowed Green's functions. We prove that the error of a perfectly matched layer decreases exponentially in comparison to the size of the window, and we also analyze the frequency of the waves of perfectly matched layers. Furthermore, in Section 4 we will be using numeric methods in order to verify the above theorems in specific cases, as well as pose conjectures related to the differences between the numerical error of windowed Green's functions and perfectly matched layers. Finally, we will summarize and pose further direction for research in this field in Section 5.

2 Preliminaries

In this section, we will be deriving the mathematical and computational basis behind our problems, including current and past techniques used to solve problems in scattering theory. Furthermore, in Subsection 2.5, we will explain the simplified problem that we analyze in our asymptotics and numerical results. Critically, in the rest of the paper, we will let $x = (x_1, x_2)$ and $y = (y_1, y_2)$ be vectors, and let $|x|$ denote the magnitude of x.

2.1 The Helmholtz Equation

In this subsection, we simplify Maxwell's wave equations to the Helmholtz equation, which is the differential equation

$$\nabla^2 f + k^2 f = 0.$$

In the rest of the paper, we analyze this simplified equation instead.

Let $\mathbf{E} = E(x, y, t)$ be a two-dimensional electric field at time t. Similarly, let $\mathbf{B} = B(x, y, t)$ be the magnetic field at every point in space at time t. From Maxwell's equations we can derive the following wave equations [15]:

$$\mu_0 \varepsilon_0 \frac{\partial^2 \mathbf{E}}{\partial t^2} - \nabla^2 \mathbf{E} = 0,$$

where μ_0 and ε_0 are respectively the permeability and permittivity of space. Similarly, for magnetism:

$$\mu_0 \varepsilon_0 \frac{\partial^2 \mathbf{B}}{\partial t^2} - \nabla^2 \mathbf{B} = 0.$$

Since the electric and magnetic wave equations are identical, we only focus our attention on the electric. Furthermore, for our problems, we assume that there is a single radiating point. This means that these equations are separable, with a single frequency ω. It is convention to write in this case that $E(x, y, t) = e^{i\omega t} f(x, y)$, and then discard the complex part. Plugging this in, we get:

$$\begin{aligned} &\nabla^2 E - \mu_0 \varepsilon_0 \frac{\partial^2}{\partial t^2} E = 0 \\ &\Leftrightarrow \nabla^2 f \cdot e^{i\omega t} - f \cdot (-\omega^2 \mu_0 \varepsilon_0 e^{i\omega t}) = 0 \\ &\Leftrightarrow \nabla^2 f + k^2 f = 0, \end{aligned}$$

where $k = \omega \sqrt{\mu_0 \varepsilon_0}$ is a constant known as the wavenumber. Furthermore, we note that radiating electric fields originating from bounded scatters (or bounded perturbations, if the metallic surface is infinite) must satisfy Sommerfeld radiation conditions. These state that for as an arbitrary point x approaches infinity, $\frac{f(x)}{\sqrt{|x|}}$ must approach zero [17]. Since the plane is uniform outside some surface Ω, as in Figure 1, we note that the permittivity and the permeability of space, and thus the wavenumber k, is the same everywhere outside Ω. Thus, the Helmholtz equation is satisfied in $\mathbb{R}^2 \setminus \Omega$.

2.2 Green's Representation Theorem

As mentioned in the introduction, Greens' representation theorem is used when performing near to far field transformations (or when solving boundary integral equations) in exterior scatter problems.

A Green's function as any function that satisfies

$$\nabla^2 G(x, y) + k^2 G(x, y) = -\delta(x - y),$$

where δ is the Dirac delta function. The function must also satisfy the Sommerfeld radiation conditions described in the previous subsection. In two dimensions, it turns out that a valid Green's function is $\frac{i}{4} H_0^{(1)}(k|x - y|)$, where $H_0^{(1)}$ is the Hankel function of the first kind, of order zero [3]. We note that

$$H_0^{(1)}(x) \sim \frac{e^{ikx}}{\sqrt{x}}$$

as x approaches infinity, which will be relevant for later work in asymptotics. Pick any, possibly infinite, surface Ω with boundary $\Gamma = \partial\Omega$. For any $x \in \Omega$, as long as the surface is uniform, we have from [3]:

$$\int_\Gamma \left(G(x,y)\frac{df(y)}{d\hat{n}} - f(y)\frac{dG(x,y)}{d\hat{n}} \right) ds_y = f(x)$$

where $\hat{n} = n(y)$ is the normal vector on the path, dependent on the point y. This theorem is incredibly powerful, as it allows us to determine the magnitude of the electric field at any point given only $f(y)$ and $\frac{df(y)}{d\hat{n}}$, i.e., the electric field and its derivative along the curve Γ. For simplicity, we define two notions known as the single and potential layer operators. We define:

$$\left[\mathcal{S}_\Gamma \varphi\right](x) = \int_\Gamma G(x,y)\varphi(y)\, ds_y$$

as the single layer operator, and

$$\left[\mathcal{D}_\Gamma \varphi\right](x) = \int_\Gamma \frac{dG(x,y)}{d\hat{n}}\varphi(y)\, ds_y$$

as the double layer operator, for any function φ and curve Γ. We can then rewrite Green's representation theorem more succinctly as

$$\left[\mathcal{S}_\Gamma \frac{\partial f}{\partial \hat{n}}\right](x) - \left[\mathcal{D}_\Gamma f\right](x) = \begin{cases} f(x) & x \in \Omega \\ 0 & \text{otherwise.} \end{cases}$$

Since Γ is often infinite, we may truncate the closed curve into a finite path Γ'. We do this by taking a finite section of the path to integrate over, and use the fact that the Green's function goes to zero at far enough points. Note that for near-to-far-field transformations we may also apply Green's representation theorem to *any* imaginary surface, as long as the plane is uniform outside the surface [3].

2.3 Windowed Green's Functions

In this subsection, we explain the mathematics behind the windowed Green's function, first described by Bruno et al. [5].

First, we define a weight function as follows. Pick a constant $0 < c < 1$ and define

$$W(t) = \begin{cases} 1 & |t| \le c \\ \exp\left(\frac{2e^{-1/u}}{u-1}\right) & |c| < t \le 1, u = \frac{|t|-c}{1-c} \\ 0 & |t| > 1. \end{cases}$$

Critically, this function is smooth at all points, and has other nice properties in relation to the asymptotics of the Green's function [1]. Now, say that we wish to apply Green's representation theorem over some infinite closed curve Γ. To do this, we must truncate the curve to some finite path Γ', and approximate (for some $x \in \Omega$):

$$f(x) = \left[\mathcal{S}_\Gamma \frac{\partial f}{\partial \hat{n}}\right](x) - \left[\mathcal{D}_\Gamma f\right](x) \approx \left[\mathcal{S}_{\Gamma'} \frac{\partial f}{\partial \hat{n}}\right](x) - \left[\mathcal{D}_{\Gamma'} f\right](x)$$

If we apply a windowed Green's function, we take the integral

$$f(x) \approx \int_{-1}^{1} \left(G(x, y(t)) \frac{df(y(t))}{d\hat{n}} - f(y(t)) \frac{dG(x, y(t))}{d\hat{n}} \right) W(t) |y'(t)| dt$$

where we have parameterized the path Γ' as a function y on $[-1, 1]$, and applied our weight to the parameterization. Analysis shows that such an error is super-algebraic in the size of the window; i.e., if $|y(1) - y(-1)|$, the length of the window, is l, then the error is $o(l^k)$ for any arbitrary real k [1].

2.4 Perfectly Matched Layers

This subsection aims to give a rough idea of a perfectly matched layer, which will be applied to imaginary surfaces in the following section.

The perfectly matched layer is inspired by the finite difference method, explained in appendix A. This method discretizes a surface, allowing a differential equation to become a system of linear equations, if all boundary conditions are known. Often, exterior boundary conditions are unknown, so we assume that boundary points at sufficiently large surfaces are zero, using the radiation condition.

However, in two dimensions, electric fields can be approximated to be $O\left(\frac{1}{\sqrt{d}}\right)$, where d is the distance from the field to the point [1]. Thus, to make sure that the electric field at far points decreases by some sufficiently large factor (say, 10^4 times smaller), we would require discretizing a space with an area 10^{16} times larger, an absurd amount of required space.

The *perfectly matched layer* artificially forces boundary points to be zero. This is done by bending the ends of the surface into the positive complex plane [10]. In our case, however, we will explain the bending in terms of Green's representation theorem, which is more useful for our purposes.

We use the asymptotics of the Green's function:

$$G(x, y) \sim \frac{e^{ik|x-y|}}{\sqrt{|x-y|}}$$

as $|x - y|$ goes to infinity (and x is fixed) [1]. It also turns out that any function f that satisfies Helmholtz must be analytic, so we can continue Green's representation theorem into the complex plane [10].

Thus, by sending $x \to x + i\sigma(x)$ on the edge of the plane, for some function $\sigma(x)$ that increases with $|x|$, we have that $|x| = \sqrt{x_1^2 + x_2^2}$ gains a positive imaginary part. If we write that $|x| = a + bi$ for positive real numbers a and b, we have

$$\frac{e^{ik|x|}}{\sqrt{|x|}} = \frac{e^{ik(a+bi)}}{\sqrt{(a+bi)}} = \frac{e^{-kba} \cdot e^{iak}}{\sqrt{(a+bi)}}$$

which decreases exponentially as b increases. Furthermore, it has been proven that b increases proportionally with σ, so the Green's function (and by extension the value we are integrating over) rapidly approaches zero [10].

2.5 Setup

For our results in future sections, we will be considering a single point source radiating outwards from $(0, 0)$. We are allowed to make this assumption because we can assume that the scattered field from an arbitrary surface can be approximated by a linear combination of radiation from the surface. In this simple case we can analytically solve to find that

$$f(x) = H_0^{(1)}(|x|)$$

where $H_0^{(1)}$ is the Hankel Function of type one and order zero. Recall that this solution satisfies

$$H_0^{(1)}(|x|) \sim \frac{e^{ik|x|}}{\sqrt{|x|}},$$

where x is any real number with sufficiently large magnitude. We will later use both the exact and asymptotic form to determine errors in our results.

3 Analytic Results

In this section, we setup and analyze asymptotic results, especially on the error function of the perfectly matched layer Green's function, which we prove has exponentially decreasing error.

3.1 Analytical Setup

Let Γ be an arbitrary infinite path, such that the plane is uniform above this path (as a real-world example, Γ might be the top side of a two dimensional waveguide). Recall Green's representation theorem in Subsection 2.2. We claim that for any x above this path, we have:

$$f(x) = \int_\Gamma \left(f \frac{dG(x,y)}{d\hat{n}} - G(x,y) \frac{df}{d\hat{n}} \right) ds_y = \left[\mathcal{S}_\Gamma \frac{\partial f}{\partial \hat{n}} \right](x) - \left[\mathcal{D}_\Gamma f \right](x)$$

This is true because $\lim_{|y|\to\infty} G(x, y) = 0$, so we can take an infinite imaginary closed curve Γ' containing Γ, such that the points on the curve are all on Γ or are at infinity.

Note that, however, it is not possible to discretize an infinite surface. Thus, we can take a finite path $L \subset \Gamma$ and write

$$f(x) \approx \left[\mathcal{S}_L \frac{\partial f}{\partial \hat{n}} \right](x) - \left[\mathcal{D}_L f \right](x)$$

In a near-to-far-field transformation, a finite difference method is applied to close points, allowing us to approximate with sufficient accuracy all points near the infinite surface (say, within some bounding box with $|x| < X$ and $|y| < Y$ for some fixed constants X and Y). We can then apply Green's representation theorem over any arbitrary surface L of our choosing, as long as this possibly infinite surface contains x, and is uniform everywhere inside the surface, as shown in Subsection 2.2.

A question may arise: given our freedom, what is the best curve to use to approximate Green's Representation Theorem? We show that in many cases, the choice of curve is irrelevant and we can take a line segment between two points.

Proposition 3.1. *Let L_1 and L_2 be differentiable paths from point a to point b. Parameterize them such that $L_1(0) = L_2(0) = a$ and $L_1(1) = L_2(1) = b$. If x is a point not contained between the paths L_1 and the line connecting a and b or between the path L_2 and the line connecting a and b, then*

$$\left[\mathcal{S}_{L_1}\frac{\partial f}{\partial \hat{n}}\right](x) - \left[\mathcal{D}_{L_1} f\right](x) = \left[\mathcal{S}_{L_2}\frac{\partial f}{\partial \hat{n}}\right](x) - \left[\mathcal{D}_{L_2} f\right](x).$$

Proof. Pick a path Ω' that is differentiable, and satisfies $\Omega'(0) = a$, $\Omega'(1) = b$, and that x is between Ω' and the line connecting a and b. Such a path exists; consider a sufficiently large ellipse that cuts off at the points a and b, for instance. Then, for $0 \leq t \leq 2$, we define:

$$\Omega_1(t) = \begin{cases} L_1(t) & 0 \leq t \leq 1 \\ \Omega'(t-1) & 1 < t \leq 2, \end{cases}$$

and similarly

$$\Omega_2(t) = \begin{cases} L_2(t) & 0 \leq t \leq 1 \\ \Omega'(t-1) & 1 < t \leq 2. \end{cases}$$

These curves are closed, and by our assumptions, x is located inside both curves. Furthermore, for $t \in [0,1]$ $\Omega_1'(t) = L_1'(t)$ and $\Omega_2'(t) = L_2'(t)$, and for $t \in (1,c)$ $\Omega_1'(t) = \Omega_2'(t) = \Omega'(t-1)$, so both curves are differentiable. Now, since x is inside both curves, we can apply Green's Representation Theorem on these curves:

$$f(x) = \left[\mathcal{S}_{\Omega_1}\frac{\partial f}{\partial \hat{n}}\right](x) - \left[\mathcal{D}_{\Omega_1} f\right](x) = \left[\mathcal{S}_{\Omega_2}\frac{\partial f}{\partial \hat{n}}\right](x) - \left[\mathcal{D}_{\Omega_2} f\right](x) \tag{1}$$

However, note that we have

$$\left[\mathcal{S}_{\Omega'}\frac{\partial f}{\partial \hat{n}}\right](x) - \left[\mathcal{D}_{\Omega'} f\right](x) = \left[\mathcal{S}_{\Omega'}\frac{\partial f}{\partial \hat{n}}\right](x) - \left[\mathcal{D}_{\Omega'} f\right](x) \tag{2}$$

Subtracting equation 1 from 2 suffices. □

To further simplify our model, we will assume that this line is parallel to the x-axis (which is the direction of the infinite side of the conductor). We can then refer to this line solely by its closest distance to the origin d, its length l, and its starting x-value x_0. Thus, we can define a function

$$F_{d,l,x_0}(x) = \left[\mathcal{S}_{L}\frac{\partial f}{\partial \hat{n}}\right](x) - \left[\mathcal{D}_{L} f\right](x)$$

where L is the line segment between (x_0, d) and (x_0+l, d). Note, by Green's representation theorem, that $F_{d,l,x_0}(x)$ approaches $f(x)$, the solution to the Helmholtz equation at a point x, when $l \to \infty$ and $x_0 \to -\infty$.

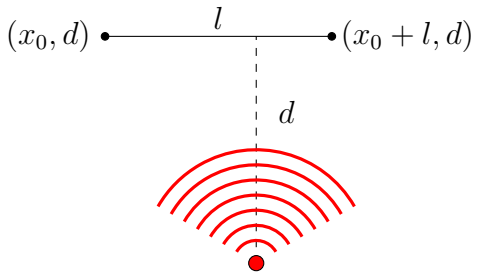

Figure 4: An illustration of the path corresponding to $F_{d,l,x_0}(x)$, with a radiating point at $(0, 0)$.

3.2 Perfectly Matched Layers on Green's Functions

In this subsection, we will explain a simple method of implementing a perfectly matched layer on an arbitrary imaginary surface, show that it is equivalent to a past method to apply perfectly matched layers to boundary integral equations, and then analyze the asymptotic errors of the method and the wavelengths of the perfectly matched layers.

First, we note that the function F defined in the previous section is additive, i.e.,

$$F_{d,l_1+l_2,x_0}(x) = F_{d,l_1,x_0}(x) + F_{d,l_2,x_0+l_1}(x)$$

In some sense, this is equivalent to "splicing" our integrating line into two separate lines. However, we claim that we can splice our line and then bend part of it into the complex plane. To do this, we add a new constant σ to our function, which is roughly the strength of our perfectly matched layer. We now define:

$$F_{d,l,x_0,\sigma}(x) = \int_L \left(f(y)\frac{dG(x,y)}{d\hat{n}} - G(x,y)\frac{df(y)}{d\hat{n}} \right) ds_y.$$

where L is the line segment from the point (x_0, d) to $(x_0 + l(1 + i\sigma), d)$. Note that this definition requires defining both magnitude and a normal vector, and we define these in as intuitively as possible. In particular,

$$|x| = \sqrt{x_1^2 + x_2^2}$$

is chosen as the root with a non-negative real part (in the rare case where $x_1^2 + x_2^2$ is a negative real number, we take it to be the root with positive imaginary part). Furthermore, the normal vector to the parametric equation $L(t)$ at some time t is defined as follows: if the derivative at t takes the form

$$L'(t) = (L_1'(t), L_2'(t)),$$

then we define the normal vector $\hat{n}$ as

$$\hat{n} = \left\langle -\frac{L_2'(t)}{\sqrt{L_1(t)^2 + L_2(t)^2}}, \frac{L_1'(t)}{\sqrt{L_1(t)^2 + L_2(t)^2}} \right\rangle$$

as the vector with length 1 that is perpendicular to the vector along the slope of the function L.

We will note that in our case, the path L is parallel to the y-axis, so the normal vector is exactly $\langle 0, 1\rangle$ everywhere along our line.

Proposition 3.2. *For any constants d, x_0 and σ and any point $x = (x_1, x_2)$ satisfying $x_1 < x_0$, we have:*

$$F_{d,\infty,x_0,\sigma}(x) = F_{d,\infty,x_0,0}(x).$$

Proof. We show that this theorem follows from a formulation of the perfectly matched layer on a boundary integral equation discovered by Lu et al. [13]. We note that our definition of magnitude is the exact same as theirs. Their paper defines a stretching of a complex plane where

$$\tilde{x}(x) = \left(x_1 + i\int_0^{x_1} \sigma_1(t)\ dt, x_2 + i\int_0^{x_2} \sigma_2(t)\ dt\right),$$

for some arbitrary functions $\sigma_1(x)$ and $\sigma_2(x)$ defined on $\mathbb{R}$. In our case, we will set $\sigma_2(x) = 0$ and

$$\sigma_1(t) = \begin{cases} 0 & x_2 < x_0 \\ \sigma & t \geq x_0. \end{cases}$$

Define $L(t) = (t, d)$ as the parameterization of the path before it gets stretched into complex space. For simplicity, define $L(\tilde{x}(x)) = \tilde{L}(x)$. In their paper, Proposition 3.2 states that if f is a solution to the Helmholtz equation $\nabla^2 f + k^2 f = 0$, then for all $x = (x_1, x_2)$ satisfying $x_1 < x_0$, we have [13]:

$$f(x) = \int_{-\infty}^{\infty} \left(\tilde{G}(x, L(t))\frac{\partial \tilde{f}(L(t))}{\partial \hat{n_c}} - \tilde{f}(L(t))\frac{\partial \tilde{G}(x, L(t))}{\partial \hat{n_c}}\right) dt.$$

where, $\hat{n_c} = \mathbf{A}^\top \hat{n}$, where $\mathbf{A} = \begin{pmatrix} \frac{1+i\sigma_2}{1+i\sigma_1} & 0 \\ 0 & \frac{1+i\sigma_1}{1+i\sigma_2} \end{pmatrix}$ and $\hat{n} = (n_1, n_2)$ is the normal vector of the real part of $\tilde{L}$. Furthermore, the functions $\tilde{G}(x, y) = G(\tilde{x}, \tilde{y})$ and $\tilde{f}(y) = f(\tilde{y})$ are defined. (Note that $\tilde{x} = x$, as $x = (x_1, x_2)$ is not in the PML.)

By Green's representation theorem:

$$f(x) = \int_{-\infty}^{\infty} \left(G(x, L(t))\frac{\partial f(L(t))}{\partial \hat{n}} - f(L(t))\frac{\partial G(x, L(t))}{\partial \hat{n}}\right) dt.$$

Furthermore, we have that $L(t) = \tilde{L}(t)$ for all $t < x_0$. Thus, by noting the integrals are equivalent for $t < x_0$, we have the following equality:

$$\begin{aligned} &\int_{x_0}^{\infty} \left(\tilde{G}(x, L(t))\frac{\partial \tilde{f}(L(t))}{\partial \hat{n_c}} - \tilde{f}(L(t))\frac{\partial \tilde{G}(x, L(t))}{\partial \hat{n_c}}\right) dt \\ =&\int_{x_0}^{\infty} \left(G(x, L(t))\frac{\partial f(L(t))}{\partial \hat{n}} - f(L(t))\frac{\partial G(x, L(t))}{\partial \hat{n}}\right) dt. \end{aligned}$$

Note that the right hand side clearly equals $F_{d,\infty,x_0,0}$. For the left hand side, we note that by chain rule:

$$\begin{aligned}\frac{\partial}{\partial \hat{n}_c}\tilde{f}(x) &= \hat{n}_c \cdot \nabla_x \tilde{f}(x) \\ &= \hat{n} \cdot (\mathbf{A}\nabla_x)\, \tilde{f}(x) \\ &= \hat{n} \cdot \nabla_{\tilde{x}} f(\tilde{x}),\end{aligned}$$

which is exactly $\frac{\partial f(\tilde{L}(t))}{\partial \hat{n}}$. Similarly, we can say that

$$\frac{\partial \tilde{G}(x, L(t))}{\partial \hat{n}_c} = \frac{\partial G(\tilde{x}, L(t))}{\partial \hat{n}}$$

which means we have that

$$\begin{aligned}&\int_{x_0}^{\infty} \left(G(x, \tilde{L}(t)) \frac{\partial f(\tilde{L}(t))}{\partial \hat{n}} - f(\tilde{L}(t)) \frac{\partial G(x, \tilde{L}(t))}{\partial \hat{n}} \right) dt \\ =&\int_{x_0}^{\infty} \left(G(x, L(t)) \frac{\partial f(L(t))}{\partial \hat{n}} - f(L(t)) \frac{\partial G(x, L(t))}{\partial \hat{n}} \right) dt.\end{aligned}$$

However, note that the first integral is exactly $F_{d,\infty,x_0,\sigma}$ and the second integral is exactly $F_{d,\infty,x_0,0}$, which suffices. □

In other words, bending any given line into the complex plane does not change the result of the evaluated Green's function integral. The reason why this is useful is very similar to the usefulness of the perfectly matching layer under finite difference methods.

Proposition 3.3. *The absolute error as the length l of the PML increases, or*

$$|F_{d,\infty,x_0,\sigma} - F_{d,l,x_0,\sigma}|,$$

is of the form $o((e^{-2k\sigma})^l)$, where σ, d, and x_0 are fixed.

Proof. We can write:

$$F_{d,\infty,x_0,\sigma} - F_{d,l,x_0,\sigma} = \int_{l+x_0}^{\infty} \left(f(y) \frac{dG(x,y)}{d\hat{n}} - G(x,y) \frac{df(y)}{d\hat{n}} \right)\, dt,$$

where $y = y(t) = (x_0 + t(1 + i\sigma), d)$. However, we know that if there is a single radiating point from $(0, 0)$, we can approximate the given solution from [1]:

$$f(x) = H_0(|x|) \approx \frac{e^{ik|x|}}{\sqrt{|x|}}.$$

Similarly, we can approximate from [1]:

$$G(x, y) = \frac{i}{4} H_0(|x - y|) = \frac{i}{4} \frac{e^{ik|x-y|}}{\sqrt{|x-y|}}.$$

We then have that

$$\nabla_y G(x,y) = e^{ik|x-y|} \cdot \left(\frac{ki}{|x-y|^{\frac{1}{2}}} - \frac{1}{2|x-y|^{\frac{3}{2}}} \right) \approx ik \frac{e^{ik|x-y|}}{\sqrt{|x-y|}}.$$

Thus, when x is fixed, we can say that

$$\left| \frac{\partial G(x,y)}{\partial \hat{n}(y)} \right| = |\hat{n}(y) \cdot \nabla_y G(x,y)| \leq |\hat{n}(y)| \cdot |\nabla G(x,y)| \approx \left| \frac{k e^{ik|x-y|}}{4\sqrt{|x-y|}} \right|.$$

Finally, note that for sufficiently large values of y, $|y| \approx |x-y|$, and $d, x_0 \ll t(1+i\sigma)$, so $|y| \approx t(1+i\sigma)$. Thus, we can compute:

$$\begin{aligned}
\left| \int_{l+x_0}^{\infty} f(y) \frac{dG(x,y)}{d\hat{n}} \, dt \right| &\leq \int_{l+x_0}^{\infty} \left| f(y) \frac{dG(x,y)}{d\hat{n}} \right| dt \\
&\approx \int_{l+x_0}^{\infty} \left| \frac{k}{4} \left(\frac{e^{ik|y|}}{\sqrt{|y|}} \right)^2 \right| dt \\
&\approx \frac{k}{4} \int_{l+x_0}^{\infty} \left| \frac{e^{2ikt(1+i\sigma)}}{t(1+i\sigma)} \right| dt \\
&< \frac{k}{4} \int_{l+x_0}^{\infty} e^{-2kt\sigma} \left| e^{2ikt} \right| dt \\
&< \frac{k}{4} \int_{x_0}^{\infty} e^{-2k(t+l)\sigma} dt \\
&= \frac{k}{4} e^{-2kl\sigma} \int_{x_0}^{\infty} e^{-2kt\sigma} dt
\end{aligned}$$

which, as we want, of the form $o(e^{-2\sigma kl})$. A very similar analysis can be performed for the other half of our integral, i.e., $-\int_{l+x_0}^{\infty} G(x,y) \frac{df(y)}{d\hat{n}} \, dt$. □

We comment that in most simulations, $|y|$ is usually substantially smaller than $|x|$; however, a very similar, though more tedious, analysis can be performed when $|y| << |x|$ to show that the error also decreases exponentially. We also note that in our case the frequency of the wave $2kt$ does not depend on σ; this is useful because higher frequency require more discretization when numerically computing the integral. Numerical experiments also show that in general, the frequency of the wave does not change substantially for varying σ.

The above error bound is also significantly better than the regular Green's function, which has an error of the form $O(l^{-\frac{1}{2}})$, and even of the windowed Green's function, which has super-algebraic error: lower than all polynomials, but larger than exponential [1].

4 Numeric Computations

In this section, we provide numerical confirmation of our propositions in Section 3, and also provide new conjectures about the comparison of accuracy between windowed Green's functions and perfectly matched layers.

4.1 Setup

As in previous section, we will assume that we are in a vacuum, with a single point source radiating outwards from $(0, 0)$. Furthermore, we fix a wave number $k = 10$. We also pick a fixed discretization for our numerical integrals with methodology described in Appendix B, at 100 points per unit length.

To use a perfectly matched layer to our advantage, we will bend the layer into the complex plane on both sides. In particular, using the propositions from the previous section, we note:

$$\begin{aligned} f(x) &= F_{d,\infty,-\infty,0}(x) \\ &= -F_{d,-\infty,a,0} + F_{d,b-a,a,0} + F_{d,\infty,b,0} \\ &= -F_{d,-\infty,a,\sigma} + F_{d,b-a,a,0} + F_{d,\infty,b,\sigma} \\ &\approx -F_{d,-z,a,\sigma} + F_{d,b-a,a,0} + F_{d,z,b,\sigma} \end{aligned}$$

for any $x = (x_1, x_2)$ with $a \leq x_1 \leq b$. Here, we set σ to be the constant 0.1, and set $d = 1$. Intuitively, what we have done here is taken a middle segment in the reals, and then bent two segments of length z on each end into the positive complex plane. For our simulations, we pick $b = 0.45l, a = -0.45l, z = 0.05l$ for a total integrating distance of l.

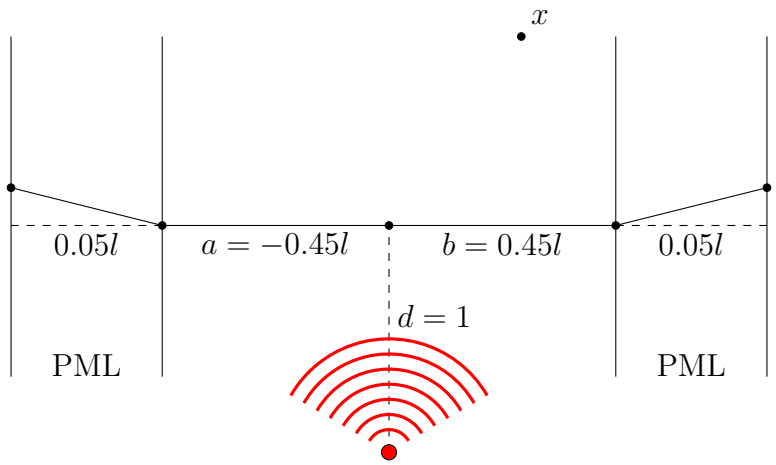

Figure 5: The standard arbitrary surface that we take, with two segments of length $0.05l$ bent into the complex plane as shown. We wish to compute the electric field at the point x.

The windowed Green's function (and regular Green's function) is implemented exactly as described in Subsection 2.3 with some truncation distance l. The path that we pick, therefore, is a line between $(-l/2, 1)$ and $(l/2, 1)$, just as the perfectly matched layer is exactly a distance 1 from the origin. We pick the constant c, as described in the subsection, to be 0.9.

Finally, we look at error evaluation. Say that we determine computationally that the field at the point x is equal to $\tilde{f}(x)$, and the true value is $f(x)$ (recall that in our experiments, this is equal to $H_0^{(1)}(|x|)$). Then our relative error, as is convention, is defined as

$$E(f, \tilde{f}) = \frac{\left|\tilde{f}(x) - f(x)\right|}{|f(x)|}.$$

4.2 Numerical Confirmations

In this subsection, we will confirm Proposition 3.2 and Proposition 3.3, by running an example perfectly matched layer. Here, we evaluate our error for the point $x = (0, 100)$.

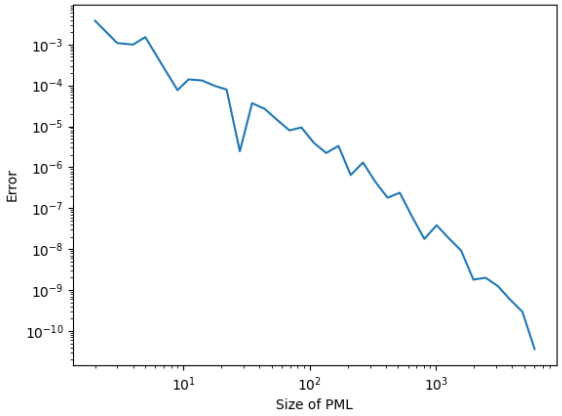

Figure 6: A plot of error with respect to the size of the PML window. Note that the error is roughly linear in the log-log plot, implying polynomial convergence order, but this is explained both because this is not asymptotic behavior and there being insufficient discretization that causes the various bumps. Recall that this is a PML layer with $\sigma = 0.1$, $d = 1$, and bending five percent of each end into the complex plane.

4.3 Comparisons Between PMLs and WGFs

In this subsection, we will do further analysis of perfect matched layers, especially by comparing them to windowed Green's functions. We will first do a generic test, by varying discretization. We will again set our test point to be $x = (0, 100)$, and say that each layer is exactly 100 units long, a distance one away from the radiating point at $(0, 0)$.

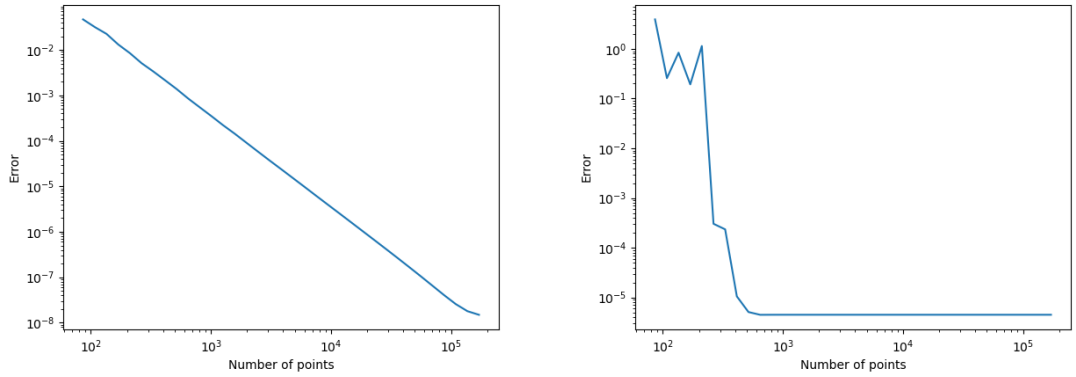

Figure 7: Perfectly matched layer on the left, windowed Green's function on the right. Notice that the windowed Green's function converges much faster than the perfectly matched layer, but with a significantly higher final error. This difference in discretization speed may be caused by the difference in the smoothness of the functions [9].

Note that perfectly matched layers, in this context, and windowed Green's functions are most effective at dealing with very far points. As such, in the next few graphs, we will set our x to be at the point $(0, x_2)$ and vary x_2, to test their relative strengths at far points.

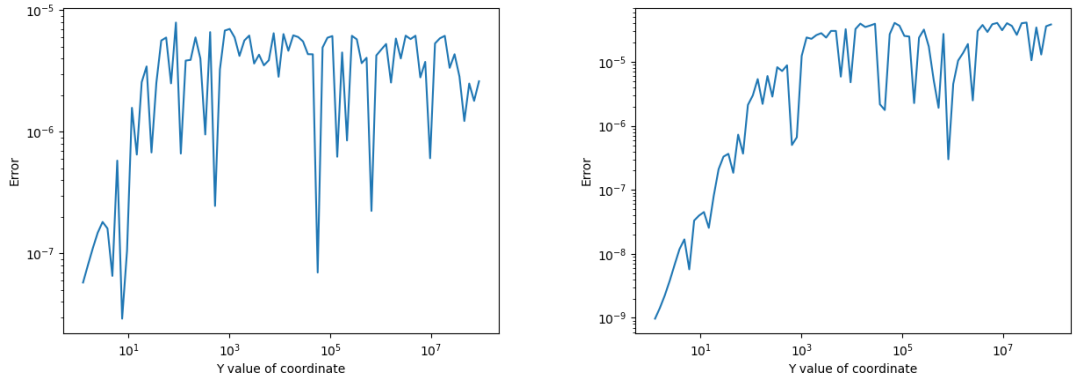

Figure 8: Perfectly matched layer on the left, windowed Green's function on the right. Both functions reach some sort of unstable limit in error as the y-coordinate increases, though the PML seems somewhat more accurate in this case. A similar pattern occurs for varying lengths of the line. We conjecture that both methods have bounded error no matter how far away the given point is.

Finally, we have noted that for the perfectly matched layer, Proposition 3.2 only holds if x is not in the complexified region. It is still possible to see whether or not the method works outside the region, however, even if errors may be higher. Thus, for $0 < \theta < \frac{\pi}{2}$, we evaluate the error at the point $x = (10^6 \sin\theta, 10^6 \cos\theta)$.

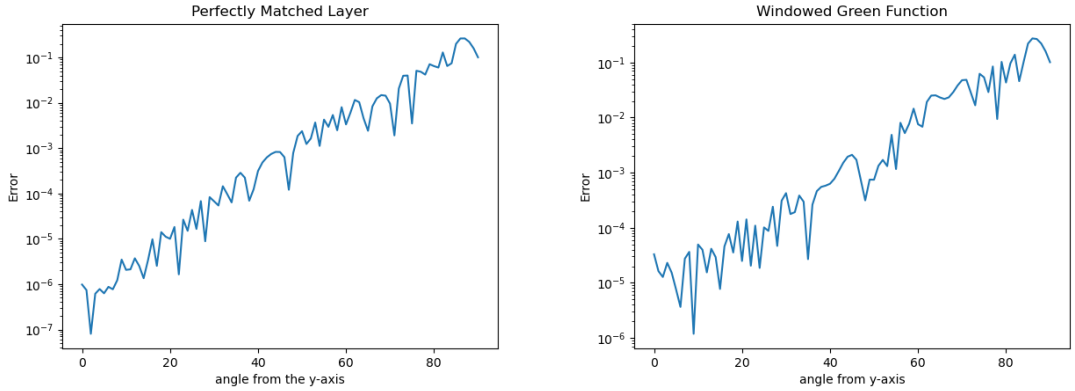

Figure 9: Perfectly matched layer on the left, windowed Green's function on the right. Both functions seem to have similar polynomially increasing error with respect to angle from the y-axis. Numeric tests indicate that a polynomially increasing error occurs even as variables, such as the distance of x from the origin, and σ, change, though further research into the slope of these graphs with respect to different variables would be interesting.

5 Conclusion

In this paper, we have described, analyzed, and compared the windowed Green's function and the perfectly matched layer on a Green's function. Analytically, we have shown that the perfectly matched layer has an error that decreases exponentially. Numerically, we have compared the perfectly matched layer and the windowed Green's function, which seem to have similar properties (though the perfectly matched layer seems significantly more accurate).

The graphs in Subsection 4.3 provide interesting areas of further research to confirm that the plots always hold, using asymptotics. In particular, formal analysis of the error values of both functions as the test point moves along the positive y-axis, as well as errors when the point rotates towards the x-axis, would be interesting to see, for further confirmation of the similarities of the two methods.

Furthermore, Figure 7 shows that perfectly matched layers require far more discretization than windowed Green's function - however, a more accurate form of numerical integration than the one described in Appendix B may significantly improve errors.

6 Acknowledgements

Thanks to Rodrigo Arrieta for being my mentor throughout this project, teaching me the background needed to complete this project, giving me guidance on this project, and giving comments on the final version of this paper. Thanks to Tanya Khovanova and Peter Gaydarov for helping me learn how to write up and present my research, as well as reviewing earlier versions of this paper. Thanks to Prof. Steven Johnson for originally proposing this topic, and meeting with me to give guidance on the later stages of this project. Finally, thanks to the Research Science Institute, for providing the opportunity and means to do this

research, along with MIT for providing the location, the Center of Excellence of Eductation and the sponsors of CEE also for making this wonderful program happen.

References

[1] Carlos Perez Arancibia. *Windowed integral equation methods for problems of scattering by defects and obstacles in layered media*. PhD thesis, California Institute of Technology, 2016.

[2] Rodrigo Arrieta and Carlos Perez-Arancibia. Windowed green function MoM for second-kind surface integral equation formulations of layered media electromagnetic scattering problems. *IEEE Transactions on Antennas and Propagation*, 70(12):11978–11989, dec 2022.

[3] Timo Beckte and Matthew Scroggs. Green's representation theorem. `https://bempp.com/handbook/theory/greens_representation.html`.

[4] Jean-Pierre Berenger. A perfectly matched layer for the absorption of electromagnetic waves. *Journal of Computational Physics*, 114(2):185–200, 1994.

[5] Oscar Bruno, Mark Lyon, Carlos Perez-Arancibia, and Catalin Turc. Windowed green function method for layered-media scattering, 2015.

[6] David L. Colton and Rainer Kress. Inverse acoustic and electromagnetic scattering theory, 2013.

[7] Wikimedia Commons. Fdtd tfsf, 2014.

[8] George Hsiao and Wolfgang L. Wendland. *Boundary Integral Equations*. Springer Berlin, Heidelberg, 2008.

[9] Steven G. Johnson. Notes on the convergence of trapezoidal-rule quadrature, 2010.

[10] Steven G. Johnson. Notes on perfectly matched layers (pmls), 2021.

[11] Randall J. LeVeque. *Finite Difference Methods for Ordinary and Partial Differential Equations*. Society for Industrial and Applied Mathematics, 2007.

[12] G.R. Liu and S.S. Quek, editors. *The Finite Element Method*. Butterworth-Heinemann, Oxford, second edition edition, 2014.

[13] Wangtao Lu, Ya Yan Lu, and Jianliang Qian. Perfectly matched layer boundary integral equation method for wave scattering in a layered medium. *SIAM Journal on Applied Mathematics*, 78(1):246–265, 2018.

[14] Wangtao Lu, Liwei Xu, Tao Yin, and Lu Zhang. A highly accurate perfectly-matched-layer boundary integral equation solver for acoustic layered-medium problems, 2022.

[15] J. Clerk Maxwell. A dynamical theory of the electromagnetic field. *Philosophical Transactions of the Royal Society of London*, 155:459–512, 1865.

[16] T.K. Sarkar and A. Taaghol. Near-field to near/far-field transformation for arbitrary near-field geometry utilizing an equivalent electric current and mom. *IEEE Transactions on Antennas and Propagation*, 47(3):566–573, 1999.

[17] A. Sommerfeld. *Partial Differential Equations in Physics*. ISSN. Elsevier Science, 1949.

Appendix

A Numerical Differentiation

In this appendix we will explain the basic theory and terminology we use when approximating derivatives. We explore these approximations primarily in relation to the Helmholtz equation. Let f be a solution to the Helmholtz equation:

$$\nabla^2 f + k^2 f = 0.$$

By Taylor series expansion, we can write that

$$f(x+h,y) - f(x,y) = h\frac{\partial f}{\partial x} + \frac{h^2}{2}\frac{\partial^2 f}{\partial x^2} + \frac{h^3}{6}\frac{\partial^3 f}{\partial x^3} + \cdots \tag{3}$$

In a very similar vein, we can write that

$$f(x-h,y) - f(x,y) = -h\frac{\partial f}{\partial x} + \frac{h^2}{2}\frac{\partial^2 f}{\partial x^2} - \frac{h^3}{6}\frac{\partial^3 f}{\partial x^3} + \cdots \tag{4}$$

However, by combining equations 3 and 4 we get that

$$f(x-h,y) + f(x+h,y) - 2f(x,y) = h^2\left(\frac{\partial^2 f}{\partial x^2} + O(h^2)\right),$$

where O is in reference to big-O notation. As such, we can approximate that

$$\nabla^2 f(x,y) = \frac{1}{h^2}\left(f(x+h,y) + f(x-h,y) + f(x,y+h) + f(x,y-h) - 4f(x,y) + O(h^2)\right).$$

By picking small h, we can numerically estimate (with high accuracy) the value of the differential equation f that satisfies the Helmholtz equation over any arbitrary surface Ω with arbitrary boundary conditions. This can be done by defining a grid of variables $X_{a,b} = f(ah, bh)$ over all integers a, b where $(ah, bh) \in \Omega$. For any a, b where (ah, bh) is inside (and not on) the boundary, we have the equation:

$$\frac{1}{h^2}\left(X_{a+1,b} + X_{a,b+1} + X_{a-1,b} + X_{a,b-1} - 4X_{a,b}\right) + k^2 X_{a,b} = 0$$

which is a system of linear equations. If boundary conditions are known, then we have a complete system of linear equations, equivalent to finding the vector v to the solution $A\vec{v} = \vec{u}$ for some square matrix A and vector u. If all boundary conditions are known precisely, the error of this method is generally sufficiently low, at $O(h^2)$ where h is the distance between consecutive points [11]. In our results, this will allow us to make many simplifications to our calculations.

In exterior scattering theory, we wish to solve this differential equation in some boundary Φ completely enclosing some conductor Ω where boundary conditions are known. We remark that as the surface Φ goes to infinity, the electric field must go to zero, allowing us to set all boundary conditions on the exterior of Φ to be zero. [1]

B Numerical Integration

In this appendix, we will also be exploring a simple method to numerically integrate a function f over any smooth path $d\Omega$ with high accuracy. In two dimensions, say that the path $d\Omega$ has a parameterization $P(t) = (x(t), y(t))$ for $0 \leq t \leq 1$. Then, we may write that

$$\int_{d\Omega} f(x)\, dx = \int_0^1 f(P(t))|P'(t)|\, dt,$$

which allows us to approximate this function as a Riemann sum:

$$\int_0^1 f(P(t))|P'(t)|\, dt \approx \frac{1}{n} \sum_{i=0}^{n-1} f\left(P\left(\frac{i}{n}\right)\right) \left|P'\left(\frac{i}{n}\right)\right|$$

for sufficiently large n. It turns out that this approximation has error about $O(n^{-2})$ for most smooth functions. However, as long as f is periodic on the interval $(0, 1)$, this approximation has *super-algebraic* error, i.e., decreasing faster than any polynomial in n, or an error of $o(n^k)$ for any k [9]. This allows us to assume in our analysis section that integrals are computed perfectly.